Anisotropy and Temperature Dependence of Myoglobin Translational Diffusion in Myocardium: Implication for Oxygen Transport and Cellular Architecture

Ping-Chang Lin, Ulrike Kreutzer, and Thomas Jue
Department of Biochemistry and Molecular Medicine, University of California Davis, Davis, California 95616-8635

ABSTRACT Pulsed field gradient NMR methods have determined the temperature-dependent diffusion of myoglobin (Mb) in perfused rat myocardium. Mb diffuses with an averaged translational diffusion coefficient (D_{Mb}) of 4.24–8.37 $\times$ 10^{-7}cm^2/s from 22°C to 40°C and shows no orientation preference over a root mean-square displacement of 2.5–3.5 μm. The D_{Mb} agrees with the value predicted by rotational diffusion measurements. Based on the D_{Mb}, the equipoise diffusion PO_2, the PO_2 in which Mb-facilitated and free O_2 diffusion contribute equally to the O_2 flux, varies from 2.72 to 0.15 in myocardium and from 7.27 to 4.24 mmHg in skeletal muscle. Given the basal PO_2 of ~10 mmHg, the Mb contribution to O_2 transport appears insignificant in myocardium. In skeletal muscle, Mb-facilitated diffusion begins to contribute significantly only when the PO_2 approaches the P50. In marine mammals, the high Mb concentration confers a predominant role for Mb in intracellular O_2 transport under all physiological conditions. The Q_{10} of the D_{Mb} ranges from 1.3 to 1.6. The Mb diffusion data indicate that the postulated gel network in the cell must have a minimum percolation cutoff size exceeding 17.5 Å and does not impose tortuosity within the diffusion root mean-square displacement. Moreover, the similar Q_{10} for the D_{Mb} of solution versus cell Mb suggests that any temperature-dependent alteration of the postulated cell matrix does not significantly affect protein mobility.

INTRODUCTION

A key tenet in respiration physiology rests on the capacity of myoglobin (Mb) to store O_2 or to facilitate O_2 transport. Although in vitro experiments have presented supporting evidence, in vivo experiments on respiring vertebrate muscle have yet to provide convincing data (1). In marine mammals, the high concentration of Mb could certainly supply O_2 during a dive or apnea (2,3). High altitude adaptation increases the expression of Mb and therefore the O_2 store (4,5). These observations agree with the tacit correlation between Mb concentration (O_2 supply) and oxidative capacity in different species (6). Yet, in spontaneously beating rat heart, Mb can prolong normal heart function for only a few seconds (7). Without any Mb, neither myocardial nor skeletal muscle function suffers any apparent impairment (8,9). The viability of an Mb-free mouse elicits two different interpretations: Mb still has a critical O_2 storage and transport function role, as evidenced by the compensating increase in capillary density. Alternatively, Mb does not have the commonly accepted O_2 storage and transport function role, and its function remains unclear.

From the vantage of facilitated O_2 diffusion, the physiology canon states that in contrast to the low solubility of O_2, the high O_2-carrying capacity of Mb confers an advantage in transporting O_2 from the sarcolemma to the mitochondria (1,10). In vitro studies have indeed confirmed that O_2 diffuses faster in Mb solution than in Mb-free solution. Mb exhibits sufficient mobility and O_2-carrying capacity to compete effectively with free O_2 (11). In vivo, however, the contribution of Mb diffusion remains uncertain, since no experiments have determined the averaged translational diffusion coefficient of myogolobin (D_{Mb}) in respiring tissue. In effect, the theory of Mb-facilitated diffusion has languished over several decades for definitive experimental confirmation.

Over the years, researchers have attempted to estimate the cellular Mb D_{Mb} by measuring Mb diffusion in concentrated solution or by following the diffusion of injected metMb in tissue homogenate or in myoglobinless frog muscle (12–14). Recent studies have taken a similar approach and have utilized fluorescence recovery after photobleaching (FRAP) technique to track injected Mb in isolated muscle (15). Observing the photooxidation of Mb in superfused rat diaphragm muscle has led to a calculated diffusion coefficient of 1.7×10^{-7} cm^2/s at 37°C (16,17). Measuring the diffusion of microinjected metMb with an attached fluorophore in isolated muscle fiber has yielded an even lower diffusion coefficient ~1.2×10^{-7} cm^2/s at 22°C (17). These reported diffusion coefficients raise questions about any significant Mb role in facilitating O_2 transport in the cell.

The FRAP results have not engendered sufficient confidence to overturn a rubric of physiology, because they do not actually measure endogenous Mb diffusion, contain an uncertain overlay of Mb oxidation/reduction kinetics in the analysis, and utilize an isolated fiber model that does not adequately mimic the physiological environment of respiring tissue (18). Moreover, the FRAP results disagree with the in vivo NMR observation of endogenous Mb rotational diffusion, which predicts a much faster translational diffusion coefficient (19,20).

Because ^{1}H-NMR studies have demonstrated the feasibility of detecting the distinct γ-CH_3 Val E11 signal of MbO_2

Submitted August 1, 2006, and accepted for publication November 6, 2006.

Address reprint requests to Dr. Thomas Jue, Biochemistry and Molecular Medicine, University of California Davis, Davis, CA 95616-8635. Tel.: 530-752-4569; Fax: 530-752-3516; E-mail: TJue@ucdavis.edu.

0006-3495/07/04/2608/13 $2.00

doi: 10.1529/biophysj.106.094458

in myocardium at −2.8 ppm, an opportunity now arises to apply a pulsed field gradient technique to map endogenous Mb translational diffusion in respiring, perfused myocardium (21,22). At 22°C, MbO_2 diffuses with an averaged coefficient of 4.24×10^{-7} cm^2/s. In contrast, solution Mb diffuses with an averaged coefficient of 11.6×10^{-7} cm^2/s. At 35°C, MbO_2 diffuses with an averaged coefficient of 7.85×10^{-7} cm^2/s and shows no orientation preference over a root mean-square (RMS) displacement of 3.4 μm. The translational diffusion coefficient matches precisely the value predicted by the NMR rotational diffusion analysis (20).

Given the reported free O_2 diffusion coefficient in the cell, a myocardium Mb concentration of 0.19 mM, and a P50 of 1.98 mmHg at 35°C, the cell reaches an equipoise diffusion PO_2 at 1.67 mmHg, where Mb and free O_2 contribute equally to the O_2 flux. Since the basal PO_2 in skeletal muscle and myocardium in vivo stands well above 10 mmHg, Mb cannot contribute significantly to the O_2 flux in the basal normoxic state (23–25).

The Q_{10} of the D_{Mb} ranges from 1.3 to 1.6 and casts a perspective on cellular architecture. In the postulated gel network model of the cell, small molecule escapes restricted diffusion by staying below a percolation cutoff size. The Mb data indicate a cutoff of at least 17.5 Å, the hydrodynamic diameter of Mb (26–28). The unrestricted Mb diffusion reveals no significant tortuosity within the RMS displacement. Moreover, the similar Q_{10} for the D_{Mb} of solution versus cellular Mb suggests that any temperature-dependent alteration or phase transition of a postulated cell matrix does not significantly affect protein mobility.

THEORETICAL BACKGROUND

NMR diffusion experiment

The effect of diffusion modifies the Bloch equation:

$$\frac{\partial \vec{M}(\vec{r},t)}{\partial t} = \gamma \vec{M}(\vec{r},t) \times \vec{B}(\vec{r},t) - \frac{M_x \hat{i} + M_y \hat{j}}{T_2} - \frac{(M_z - M_0)\hat{k}}{T_1} + \nabla D(\vec{r}) \cdot \nabla \vec{M}(\vec{r},t), \quad (1)$$

where γ is the magnetogyric ratio. The first three terms on the right correspond to the general Bloch equation; the last term, $\nabla D \cdot \nabla \vec{M}$, reflects the effect of diffusion in anisotropic medium, first shown by Torrey (29). Its solution, based on the NMR diffusion experiment, requires measurements of the echo amplitude $S(G)$ as a function of the applied field gradient $G(t)$. The analysis utilizes the following equation (30):

$$\ln\left(\frac{S(G)}{S(0)}\right) = -\gamma^2 \int_0^\tau \left[\int_0^{t'} \vec{G}(t'')dt'\right] \times D \times \left[\int_0^{t'} \vec{G}(t'')dt''\right]^T dt' = -\sum_{i=1}^{3}\sum_{j=1}^{3} b_{ij} D_{ij}, \quad (2)$$

where $S(0)$ is the intensity of echo with no gradient, $S(G)$ is the intensity of echo with the applied field gradient, G is the applied field gradient, τ is the echo time, $\boldsymbol{D}$ is the 3×3 rank-two diffusion tensor, D_{ij} is an element of the tensor $\boldsymbol{D}$, and b_{ij} is the element of the 3×3 matrix $\boldsymbol{b}$

$$b = \gamma^2 \int_0^\tau \left[\int_0^{t'} \vec{G}(t'')dt''\right]^T \times \left[\int_0^{t'} \vec{G}(t'')dt''\right] dt', \quad (3)$$

in which $G(t) = [G_x(t), G_y(t), G_z(t)]$, a field gradient vector. According to Eqs. 2 and 3, the diffusion experiments can be designed to observe different linear combinations of the components of $\boldsymbol{D}$ by applying field gradients along various oblique directions. For well-described anisotropic diffusion, no less than seven experiments are required to evaluate all diagonal and off-diagonal elements of the symmetrical 3×3 matrix $\boldsymbol{D}$ and $S(0)$ (31).

Specifically, pulsed field gradient spin echo (PGSE) or pulsed field gradient stimulated echo (PGSTE) sequences can determine the self-diffusion coefficients (30). However, the utilization of rectangular gradient pulses generates significant eddy current, which is proportional to dI/dt. Decreasing the rate of change in the gradient pulses reduces the eddy current. Trimming the $\boldsymbol{G}$(t) gradient pulse utilizes ramp functions to create a modified pulse train (Fig. 1). The time intervals are as follows:

Functional forms of $G(t)$ in the serial time subintervals

Pulse sequence subinterval t	Ramped rise and fall of $G(t)$
$0 < t \le t_1$	0
$t_1 < t \le t_1 + \varepsilon$	$G_{sin}(t - t_1)\pi/2t$
$t_1 + \varepsilon < t \le t_1 + \delta$	G
$t_1 + \delta < t \le t_1 + \delta + \varepsilon$	$G_{sin}(t - t_1 - \delta)\pi/2\varepsilon + \pi/2$
$t_1 + \delta + \varepsilon < t \le t_1 + \Delta$	0
$t_1 + \Delta < t \le t_1 + \Delta + \varepsilon$	$G_{sin}(t - t_1 - \Delta)\pi/2\varepsilon$
$t_1 + \Delta + \varepsilon < t \le t_1 + \Delta + \delta$	G
$t_1 + \Delta + \delta < t \le t_1 + \Delta + \delta + \varepsilon$	$G_{sin}((t - t_1 - \Delta - \delta)(\pi/2\varepsilon + \pi/2))$
$t_1 + \Delta + \delta + \varepsilon < t \le \tau$	0

Adjusting for the nonrectangular gradient pulses yields a modified equation for b_{ij}.

$$b_{ij} = \gamma^2 G_i G_j \left[\frac{4(3\pi - 26/3)\varepsilon^3}{\pi^3} + (\Delta - \delta - \varepsilon)\left(\delta + \left(\frac{4}{\pi} - 1\right)\varepsilon\right)^2 + \frac{1}{3}\left(\delta - \varepsilon\left(1 - \frac{2}{\pi}\right)\right)^3 + \frac{2\varepsilon(\pi^3\delta^2 + 2\pi\delta\varepsilon(4 - \pi(\pi - 2)) + \varepsilon^2(16 + \pi^3 - 4\pi^2 - 2\pi))}{\pi^3} + \frac{1}{3}\left(\left(\delta + \left(\frac{2}{\pi} - 1\right)\varepsilon\right)^3 - \frac{8\varepsilon^3}{\pi^3}\right)\right]. \quad (4)$$

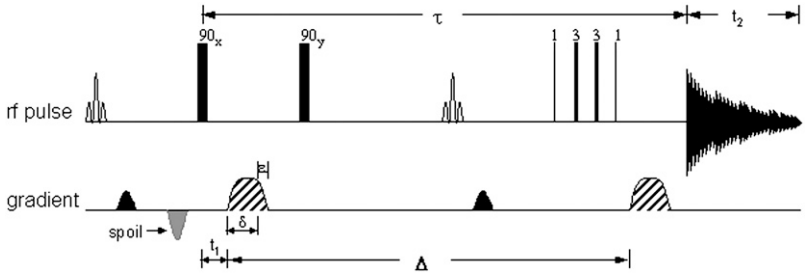

FIGURE 1 The modified PGSTE sequence in the NMR diffusion measurements used two modified CHESS pulse sequences (one inserted in front of the first 90° pulse and the other one located between the second 90° pulse. The binomial pulse suppress the water and fat signals. The 1331 binomial pulse excite selectively the γ-CH_3 Val E11 signal of MbO_2 (or MbCO).

In the case of isotropic diffusion, the observations corresponding to the diagonal elements of $\boldsymbol{D}$ will not differ. All off-diagonal elements, however, will vanish.

O_2 diffusion in muscle cell

Oxygen transport from the sarcolemma to the mitochondria has contributions from free O_2 and Mb-facilitated diffusion, as expressed in the following equation (11,18):

$$fO_2 = fO_2^{\mathrm{Mb}} + fO_2^{\mathrm{O_2}} = \left(K_0 + D_{\mathrm{Mb}}C_{\mathrm{Mb}}\frac{dS}{d(PO_2)}\right)\frac{d(PO_2)}{dx} = \left(K_0 + D_{\mathrm{Mb}}C_{\mathrm{Mb}}\frac{P50}{(PO_2+P50)^2}\right)\frac{d(PO_2)}{dx}, \quad (5)$$

where PO_2 = partial pressure of O_2, fO_2 = O_2 flux density, fO_2^{Mb} = O_2 flux density from Mb, $fO_2^{\mathrm{O_2}}$ = O_2 flux density from free O_2, K_0 = Krogh's diffusion constant for free O_2, D_{Mb} = Mb diffusion coefficient, C_{Mb} = Mb concentration, $S = (PO_2/PO_2{+}P50)$ = fraction of Mb saturated with O_2. P50 = the PO_2 that half saturates Mb, which reflects the O_2-binding affinity of Mb. The overall Mb-facilitated and free O_2 flux in the cell requires the integration of the MbO_2 and O_2 distribution, which in turn depends upon the PO_2 gradient between the sarcolemma and the surface of mitochondria. Integrating Eq. 5 with the mitochondria PO_2 boundary condition assumed as 0 mmHg and with the sarcolemma to mitochondria distance along X set as unit length yields $FO_2^{\mathrm{O_2}} = K_0PO_2$ for the free O_2 flux and $FO_2^{\mathrm{Mb}} = D_{\mathrm{Mb}}C_{\mathrm{Mb}}(PO_2/(PO_2{+}P50))$ for the Mb-facilitated O_2 diffusion. Mb-facilitated diffusion of O_2 depends upon PO_2, C_{Mb}, and P50. Equation 6 then describes the relative Mb-facilitated versus free O_2 flux

$$\frac{FO_2^{\mathrm{Mb}}}{FO_2^{\mathrm{O_2}}} = \frac{\int_0^{\mathrm{PO_2}} fO_2^{\mathrm{Mb}}d(PO_2)}{\int_0^{\mathrm{PO_2}} fO_2^{\mathrm{O_2}}d(PO_2)} = \frac{D_{\mathrm{Mb}}C_{\mathrm{Mb}}}{K_0(PO_2+P50)}. \quad (6)$$

When $(FO_2^{\mathrm{Mb}}/FO_2^{\mathrm{O_2}}) = 1$, Mb-facilitated O_2 and free O_2 contribute equally to the O_2 flux. The associated PO_2 is defined as the equipoise diffusion PO_2.

MATERIALS AND METHODS

Protein preparation

Mb solution was prepared from lyophilized horse heart protein (Sigma Chemical, St. Louis, MO). The preparation of MbO_2 and MbCO solution followed the procedure described previously (32).

Animal preparation and heart perfusion

The procedure for rat heart perfusion was performed as previously described (33,34). Male Sprague-Dawley rats (350–400 g) were anesthetized by an intraperitoneal injection of sodium pentobarbital (65 mg/kg) and heparinized (1000 units/kg) by injection into the femoral vein. The heart was quickly isolated and placed in ice cold buffer solution until aortic cannulation, followed by perfusion in Langendorff mode with Krebs-Henseleit buffer containing (in mM) 118 NaCl, 4.7 KCl, 1.2 KH_2PO_4, 1.8 $CaCl_2$, 23 $NaHCO_3$, 1.2 $MgSO_4$, 15 glucose. The perfusate was maintained by a peristaltic pump (Rainin, Oakland, CA) at a constant, nonrecirculating perfusion flow of 12–19 ml/min and at the respective temperatures. Perfusion pressure was measured with a pressure transducer (Medex, Hilliard, OH) via a Y-connection in the aortic cannula. A saline-filled latex balloon inserted in the left ventricle monitored the heart rate (HR) and left ventricular pressure (LVP) via a second pressure transducer. Both transducers were connected to a Biopac (Goleta, CA) recording system. The balloon volume was adjusted to give an end-diastolic pressure of 4–6 mmHg. Rate pressure products were calculated from HR × the left ventricular developed pressure (LVDP). The perfusate was gassed with 95% O_2, 5% CO_2 and was passed through a 5-μm and a 0.45-μm Millipore filter. The perfusate temperature was maintained with a heat-regulated circulating water bath and water-jacketed reservoirs and tubings. A microthermocouple inserted into the left ventricle calibrated the buffer temperature, heater output, and thermal sensor to maintain the tissue at a defined temperature of 22°C, 30°C, 35°C, or 40°C. All target temperatures have a deviation of $<\pm1$°C.

K^+ arrest

After a 20-min control period the perfusate was switched to Krebs-Henseleit buffer containing 92.7 mM NaCl and 30 mM KCl. Other buffer components remained the same, as listed above. With 30 mM KCl, the heart stopped beating. Ten minutes after the heart stopped beating, the perfusate flow rate was reduced to 50% of control. Heating power was readjusted because of the reduction of flow rate. High K^+ perfusion continued for ~4–6 h, which depended upon the experiment at different temperature. The perfusate was then switched back to 118 mM NaCl, 4.7 mM KCl, and the flow returned to its control level. Perfusion continued then for 20–30 min.

NMR

An Avance 400-MHz Bruker (Billerica, MA) spectrometer measured the $^1H/^{31}P$ signals with a 20-mm microimaging gradient probe. The ^1H 90° pulse, calibrated against the H_2O signal from a 0.15 M NaCl solution or perfusate, was 65 μs. A modified Stejskal-Tanner PGSE or PGSTE sequence followed the Val E11 resonance of MbCO and MbO_2 at −2.4 ppm and −2.8 ppm, respectively (22,35,36). The gradient field strength ranged from 0 to 95 G (G/cm). A typical spectrum required 1024 scans and used the following signal acquisition parameters: 8,192-Hz spectral width, 4,096 data points, and 255-ms acquisition time. Zero-filling the free induction decay and apodizing with an exponential-Gaussian window function improved the spectra. A spline fit then smoothed the baseline. The H_2O line served as the spectral reference, 4.75 ppm at 25°C relative to sodium-3-(trimethylsilyl)propionate-2,2,3,3-d4 at 0 ppm.

Diffusion measurements in perfused heart experiments utilized a modified PGSTE sequence that included chemical shift selective (CHESS) pulses (37). One CHESS pulse suppressed the water signal; the other CHESS pulse, inserted between the second and third 90° pulses, attenuated the fat signal at 1 ppm. The trapezoidal pulsed field gradients with various magnitudes and directions were applied to measure diffusion coefficients in different orientations. In addition, a 1331 pulse replaced the third 90° pulse. For the diffusion measurements, the acquisition parameters included the following: acquisition time, 38.5 ms; spectral width, 10 KHz; data points, 768. A typical spectrum required 16,000 transients or ~24 min of signal accumulation. The PGSTE, as illustrated in the pulse train diagram, had the following intervals: $\Delta = 24$ ms, $\delta = 2.4$ ms, $\varepsilon = 0.6$ ms, and $\tau = 27.5$ ms.

Seven non-co-linear pulsed field gradient directions $\boldsymbol{G} = (G_x, G_y, G_z)$ were selected to measure the diffusion tensor components (31). In each direction, the gradient strength, G_i, was 0 or increased incrementally from 18.2 G/cm to 73.0 G/cm in 18.3 G/cm steps.

For the ^{31}P spectra, the signal acquisition utilized a 55° pulse angle, 6494-Hz spectral width, 4096-point data size, and 0.65-s repetition time. The ^{31}P 90° pulse was 72 μs, calibrated against a 0.1 M phosphate solution. All ^{31}P signals were referenced to PCr peak as 0 ppm. A typical spectrum required 256 scans. The PCr/ATP ratio was corrected by a scaling factor calculated from fully relaxed spectra.

Statistical analysis

Statistical analysis used the Sigma Plot/Sigma Stat program (Systat Software, Point Richmond, CA) and expressed the data as mean ± SE. Linear least squares regression analysis of the individual data points determined the slopes, intercepts, and correlation coefficients. Statistical significance was determined by two-tailed student's *t*-test, $P < 0.05$. For evaluating the six independent components of the self-diffusion tensor, the method of multivariate linear regression was utilized to estimate the regression parameters of the system of linear equations. All regression analyses used primary data points and the ANOVA statistics for the regression and the corresponding *F* test value for each step.

RESULTS

The perfused rat myocardium shows physiological characteristics consistent with previous literature reports (33,34). Introducing 30 mM KCl stops heart contraction and removes any cardiac motional artifact from the diffusion measurements. At 35°C, K^+ induces a rate pressure product (RPP) drop from 27.5 ± 1.7 × 10^3 mmHg min^{-1} to zero. During the K^+ arrest period, MVO_2 reduces from 26.8 ± 2.0 to 7.3 ± 1.2 μmol min^{-1} g^{-1} dry weight (dw); ATP declines to 93.0% ± 3.7% of control. PCr decreases to 95.5% ± 3.8% of the basal level. During reperfusion with K^+ free, control state buffer, MVO_2 returns to 30.6 ± 3.5 μmol min^{-1} g^{-1} dwt. ATP and PCr recover to 83.6% ± 3.1% and 84.9% ± 3.5% of the control level. RPP returns to 28.1 ± 1.5 × 10^3 mmHg min^{-1}. Table 1 summarizes the physiological parameters from 22°C to 40°C.

Fig. 1 displays the NMR pulse sequence used to detect the Mb signal. Fig. 2 shows the ^{1}H-stacked spectra of the Val E11 γ-methyl signal of MbO_2 at −2.8 ppm from perfused myocardium at 30°C. The measurement utilizes a modified PGSTE sequence at different gradient fields applied in the X-direction. At 0.9 G/cm, the Val E11 γ-methyl signal of MbO_2 shows the highest signal intensity (Fig. 2 *A*). For trace B to E, the signal intensity decreases incrementally as the gradient strength increases stepwise from 18.2 G/cm to 73.0 G/cm.

For the perfused rat myocardium at 22°C, the apparent diffusion tensor, $\boldsymbol{D}$, estimated by a set of seven non-co-linear pulsed field gradients, is shown with its standard error matrix below:

$$D = \left[\begin{pmatrix} 4.47 & 0.35 & 0.02 \\ 0.35 & 4.47 & 0.33 \\ 0.02 & 0.33 & 4.53 \end{pmatrix} \pm \begin{pmatrix} 1.78 & 0.58 & 0.55 \\ 0.58 & 2.07 & 0.51 \\ 0.55 & 0.51 & 1.96 \end{pmatrix} \right] \times 10^{-7}\ \mathrm{cm}^2/\mathrm{s}. \quad (7)$$

The correlation coefficient $R = 0.725$.

TABLE 1 Physiological parameters for perfused heart

	LVDP (mmHg)	HR (min^{-1})	RPP (mmHg min^{-1} × 10^3)	MVO_2 (μmol min^{-1} g^{-1} dwt)	PCr (%)	ATP (%)	PCr/ATP ratio	pH	*n*
				22°C					
Control	150.9 ± 7.2	72.3 ± 2.6	10.9 ± 0.4	14.1 ± 0.6	100	100	1.75 ± 0.04	7.18 ± 0.03	6
K^+ Arrest	n/a	0	0	5.0 ± 0.4*	120.6 ± 4.3*	95.4 ± 1.6	2.28 ± 0.10	7.22 ± 0.02	6
Reperfusion	148.9 ± 8.4	71.0 ± 4.6	10.5 ± 0.7	14.6 ± 1.0	93.2 ± 3.2	93.9 ± 1.3	1.75 ± 0.12	7.19 ± 0.03	6
				30°C					
Control	133.4 ± 7.8	173.1 ± 11.3	22.8 ± 1.5	20.1 ± 26	100	100	1.37 ± 0.11	7.19 ± 0.00	5
K^+ Arrest	n/a	0	0	4.3 ± 0.6*	106.2 ± 2.6*	101.2 ± 1.8	1.43 ± 0.09	7.20 ± 0.00	5
Reperfusion	134.8 ± 9.4	177.8 ± 12.1	23.5 ± 1.7	21.4 ± 2.5	88.5 ± 3.8*	96.9 ± 3.7	1.24 ± 0.05	7.19 ± 0.01	5
				35°C					
Control	118.3 ± 5.0	231.5 ± 7.69	27.5 ± 1.7	26.8 ± 2.0	100	100	1.39 ± 0.07	7.17 ± 0.01	8
K^+ Arrest	n/a	0	0	7.3 ± 1.2*	95.5 ± 3.8	93.0 ± 3.7	1.36 ± 0.04	7.19 ± 0.01	8
Reperfusion	125.4 ± 6.4	222.2 ± 7.4	28.1 ± 1.5	30.6 ± 3.5	84.9 ± 3.5*	83.6 ± 3.1	1.34 ± 0.04	7.14 ± 0.01	8
				40°C					
Control	127.7 ± 10.9	294.4 ± 16.4	36.8 ± 5.7	33.5 ± 4.6	100	100	1.28 ± 0.07	7.12 ± 0.01	4
K^+ Arrest	n/a	0	0	9.7 ± 2.4*	103.7 ± 5.3	94.4 ± 0.5*	1.40 ± 0.10	7.15 ± 0.01	4
Reperfusion	130.9 ± 12.3	294.2 ± 26.3	37.4 ± 5.1	34.1 ± 3.2	76.0 ± 2.4*	87.2 ± 5.1*	1.12 ± 0.06	7.10 ± 0.02	4

LVDP, left ventricular developed pressure; HR, heart rate; RPP, rate pressure product; PCr, phosphocreatine.
*Indicates statistical significance.

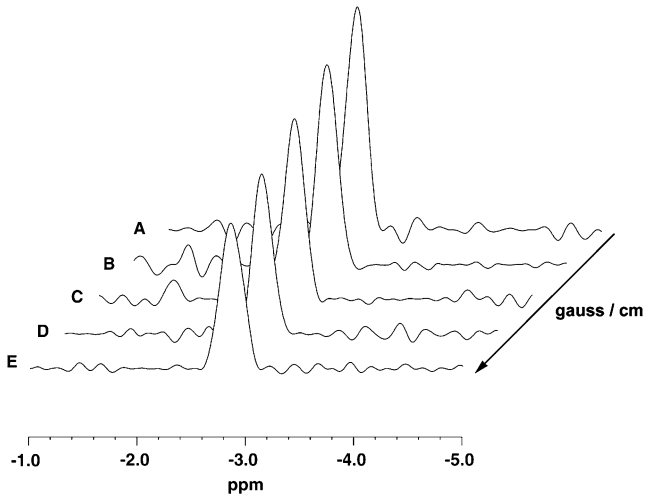

FIGURE 2 ^{1}H-NMR diffusion-weighted spectra of MbO_2 from perfused rat heart under K^+ arrest at 30°C: A modified pulse PGSTE sequence detects the γ CH_3 Val E11 signal at −2.8 ppm. The peak intensity changes as a function of gradient field strength in the X direction: (*A*) 0.9 G/cm, (*B*) 18.2 G/cm, (*C*) 36.5 G/cm, (*D*) 54.7 G/cm, and (*E*) 73.0 G/cm.

In addition, to investigate if the diffusion tensor $\boldsymbol{D}$ is an isotropic matrix, a null hypothesis of isotropic diffusion, $\boldsymbol{D} = D_0\boldsymbol{I}$, is applied. Assuming that the null hypothesis is true, the diffusion tensor is $D = (5.22 \pm 0.57) \times 10^{-7}\ I$ (cm^2/s), estimated from the same data set. $R = 0.717$.

F distribution examines whether the null hypothesis is acceptable, using the relevant F equation

$$F = \frac{(SS_c - SS_u)/(DF_u - DF_c)}{SS_c/[N - (DF_u + 1)]}, \tag{8}$$

where SS_c and SS_u are the residual sum of squares due to regression in the constrained and unconstrained models, respectively; DF_u represents the regression degrees of freedom in the unconstrained model as well as DF_c does in the constrained model, and N is the total number of data points. Given $DF_u = 6$, $DF_c = 1$, and $N = 79$ in this experiment, the value of F is 0.31 according to Eq. 8, which is smaller than $F[DF_u - DF_c, N - (DF_u + 1)] = 3.30$ and 2.35 for the 1% and 5% confidence limits, respectively; therefore, the null hypothesis of isotropic diffusion is accepted. Given the isotropic diffusion at 22°C, a restricted time window to maintain a viable perfused myocardium above 30°C, and an extended signal acquisition time required to achieve sufficient signal to noise, the experiments at 30°C and 35°C have only investigated Mb diffusion with applied field gradients in three orthogonal directions.

TABLE 2 Mb translational diffusion in myocardium at different temperatures

Gradient direction	D_{Mb} ($\times 10^{-7}$ cm^2/s) at different temperatures			
	22°C	30°C	35°C	40°C
X	4.12 ± 0.32	6.18 ± 0.65	7.97 ± 1.03	
Y	4.51 ± 0.38	6.07 ± 1.00	7.76 ± 0.68	
Z	4.08 ± 0.19	6.07 ± 0.64	7.85 ± 0.79	
Averaged D^*_{Mb}	4.24 ± 0.25*	6.09 ± 0.45*	7.85 ± 0.49*	8.37 ± 0.37†

*The translational diffusion coefficients were obtained by analyzing all the data points collected in all gradient directions to run statistics tests ($n = 75$ at 22°C, 72 at 30°C, and 60 at 35°C).

†The self-diffusion coefficient of Mb at 40°C was measured in one gradient direction, XY (45° between X and Y directions) only.

Fig. 3 shows the natural logarithm of the MbO_2 signal intensity from perfused hearts ($n = 5$) as a function of b (Eqs. 3 and 4) from 22°C to 40°C. The slope of the graph leads to the determination of the translational diffusion coefficient. Applying the gradient field along X, Y, or Z does not produce any significant deviations in the slopes under all temperature conditions, consistent with isotropic diffusion. Table 3 lists the temperature-dependent diffusion coefficients.

Fig. 4 shows a linear relationship between the averaged value of the diffusion coefficient D and temperature. The slope of the linear regression line, 2.41×10^{-8} cm^2/s °C, depicts a 73.8% increase in D from 22°C to 35°C, corresponding to the temperature coefficient (Q_{10}) of 1.53. In addition, the temperature coefficient calculated from D at any two temperature points ranges between 1.3 and 1.6, which agrees with literature values. The Q_{10} of cellular MbO_2 diffusion agrees with previous literature reports and the Q_{10} of 1.31 observed in solution MbO_2 (Tables 3 and 4).

Fig. 5 compares the relative O_2 flux contribution of free O_2 transport with Mb-facilitated diffusion. Free O_2 flux has a linear dependence on K_0, the Krogh's diffusion coefficient, whereas Mb-facilitated O_2 diffusion has a nonlinear dependence on D_{Mb} and P50. As temperature rises from 22°C to 40°C, K_0 increases from 2.52 to 4.81×10^{-5} ml O_2 $cm^{-1} \times min^{-1} \times atm^{-1}$ (38); D_{Mb} increases from 4.24 to 8.37×10^{-7} $cm^2 s^{-1}$. The equipoise diffusion PO_2 changes with only a modest temperature dependence. Mb-facilitated diffusion begins to dominate the O_2 flux below the equipoise diffusion PO_2. Table 5 summarizes the equipoise diffusion PO_2 values at different D, K_0, and temperatures. Altering the temperature from 22°C to 40°C changes the equipoise diffusion PO_2 from 2.72 to 0.15 mmHg in myocardium and 6.67 to 4.24 mmHg in skeletal muscle.

Fig. 6 maps the hyperbolic relationship between K_0 and (PO_2 + P50), given C_{Mb} of 0.19 mM for Mb and D_{Mb} at different temperatures (see Table 2) based on the relationship $(FO_2^{Mb}/FO_2^{O_2}) = (D_{Mb}C_{Mb}/K_0(PO_2+P50)) = 1$. At the equipoise diffusion PO_2, $K_0 = (D_{Mb}C_{Mb}/(PO_2+P50))$. As the P50 value increases, the free O_2 flux required to match Mb-facilitated diffusion decreases. Temperature also alters the D_{Mb} and the P50 and will introduce a new set of curves.

DISCUSSION

Physiological model

The K^+-arrested perfused rat myocardium provides a convenient physiological model to interrogate endogenous Mb

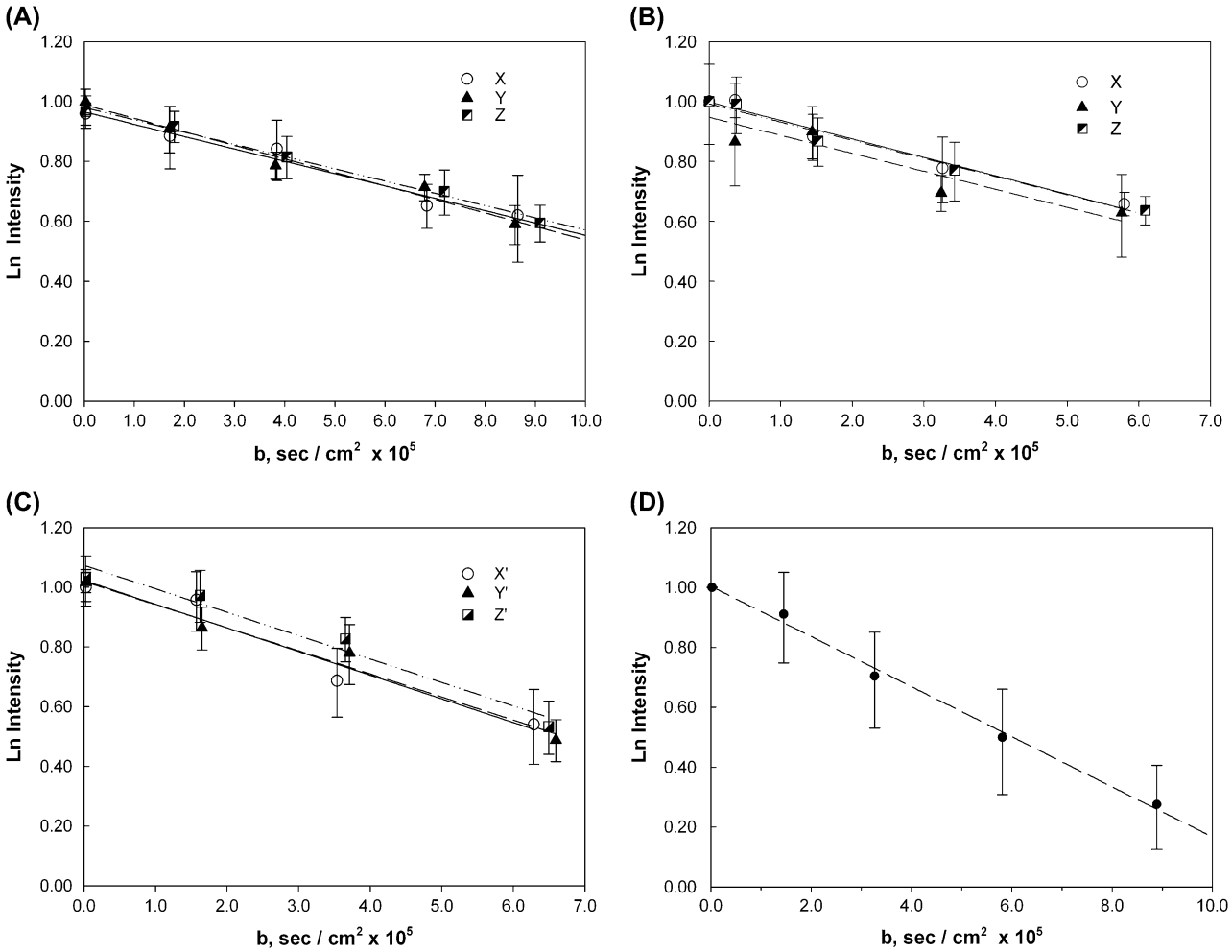

FIGURE 3 Plots of the natural logarithm of the MbO_2 Val E11 peak intensity at different temperatures as a function of **b**: The MbO_2 signals reveal decreasing the intensity with each stepwise increase in gradient field strength applied along the X, Y, and Z directions. The translational diffusion coefficients are as follows: (*A*) 22°C: 4.12, 4.51, and 4.08 $\times$ 10^{-7} cm^2/s ($n = 5$), (*B*) 30°C: 6.18, 6.07, and 6.07 $\times$ 10^{-7} cm^2/s ($n = 5$), (*C*) 35°C: 7.97, 7.76, and 7.85 $\times$ 10^{-7} cm^2/s ($n = 5$), and (*D*) 40°C: 8.37 $\times$ 10^{-7} cm^2/s in the XY direction ($n = 4$). The standard error on each point was calculated from five (or four) different perfused heart measurements. In addition, the regression lines for the respective data points show no significant difference at any measuring temperature from 22°C to 35°C.

diffusion. Under control conditions without K^+ at physiological temperature of 35°C, RPP (27.5 $\pm$ 1.7 mmHg $min^{-1} \times 10^3$), MVO_2 (26.8 $\pm$ 2.0 μmol min^{-1} g^{-1} dwt), and other metabolism parameters agree with literature reports of saline-perfused rat myocardium (33,34). Introducing 30 mM KCl stops the heart contraction and removes cardiac motion artifact from the diffusion measurements. Even though RPP falls to zero, MVO_2 continues at 27% of its control level (7.3 $\pm$ 1.2 μmol min^{-1} g^{-1} dwt) and maintains the heart at a high energy charge (39). The noncontractile energy demand of the heart consumes ATP at a rate of 21.9 μmol min^{-1} g^{-1} dwt, assuming a P/O ratio of 3:1. During recovery from K^+ arrest, MVO_2 (30.6 $\pm$ 3.5 μmol min^{-1} g^{-1} dwt) and RPP (28.1 $\pm$ 1.5 mmHg $min^{-1} \times 10^3$) return to their respective control levels. PCr and ATP also approach their respective control levels. The slight deviation from full PCr and ATP recovery requires additional experiments to clarify but does not impair the use of the K^+-arrested perfused heart in investigating Mb diffusion in the cell (7). At all temperatures 22°C–40°C, the hearts exhibit previously observed physiological and metabolic profiles.

Cellular Mb

The detectable NMR signal of the MbO_2 Val E11 signal in myocardium and skeletal muscle presents an opportunity to investigate the endogenous D_{Mb} in the cell with pulsed field gradient techniques. Using the NMR data to quantitate the translational diffusion coefficient requires defining two premises: Mb visibility and O_2 heterogeneity.

A significant pool of bound Mb would complicate the diffusion analysis. Comparative in vitro and in vivo experiments, however, indicate an entirely free, mobile, and NMR-detectable pool of Mb. ^{1}H-NMR spectral analysis of

TABLE 3 Diffusion coefficients of Mb in solutions and in muscles

Sample	Method	$D_{Mb} \times 10^{-7}$ cm^2/s	Q_{10} [T_1, T_2], °C	°C	Reference
MbCO solution (1.8 mM)	NMR	11.6		22	This work
		16.5	1.31 [22, 35]	35	This work
MbO_2 solution (1.8 mM)	NMR	11.6		22	This work
Mb diluted solution	Diffusion tube	11.3		20	(12)
Mb diluted solution in capillary	Photobleaching	9.9		22	(16,17)
		14.8	1.31 [22, 37]	37	(16,17)
Mb in rat myocardium	Perfused heart, NMR	4.24		22	(74)
		7.85	1.61 [22, 35]	35	This work
Isolated rat soleus muscle fiber	Microinjection of metMb, photobleaching	1.2		22	(16,17)
		2.2	1.50 [22, 37]	37	(16,17)
Isolated rat cardiac muscle fiber	Microinjection of metMb, photobleaching	1.1		22	(16,17)
		1.7	1.49 [22, 37]	37	(16,17)
Mb in undiluted homogenates of rat skeletal muscle	Multilayer diffusion	1.5		20	(14)
Injected Mb in frog skeletal muscle	Microinjection of Mb, fluorescence, and photooxidation	2.7	1.41 [20, 37]	37	(14)
		1.6	1.60 [16, 22]	22	(13)

Q_{10} is the relative change in the diffusion coefficient corresponding to 10°C change in temperature as defined by $Q_{10} = (D_2/D_1)^{(10/(T_2-T_1))}$.

the in situ Mb signal and biochemical assay of the tissue yield matching concentration values for Mb. Moreover, the Val E11 signal line shape in the cell versus in solution shows no significant deviation (32). Mb appears to diffuse freely in cell. No significant compartmentalization exists.

Any O_2 heterogeneity can also pose an analysis hurdle, since the Val E11 signal intensity corresponds directly to the oxygenation level. Under normoxic conditions, the perfused myocardium model in this study reveals no sign of O_2 heterogeneity, which would give rise to a regional distribution of partially saturated MbO_2 (40). Infusing high affinity CO into perfused myocardium produces an equivalent MbCO Val E11 signal intensity. The MbCO signal intensity never exceeds the corresponding one from MbO_2, and the total integrated signal area remains constant (36,41). Any O_2 heterogeneity would yield a higher MbCO signal intensity. Even though some investigators have reported O_2 heterogeneity in the perfused heart, these contrasting observations arise most likely from differences in the experiment model (42).

Given these premises, the diffusion analysis yields diffusion coefficients of solution state of dilute Mb (11.6×10^{-7} cm^2/s) and Hb (7.53×10^{-7} cm^2/s), which agree with literature values (Table 3). In myocardial tissue at 35°C, Mb diffusion decreases from 16.5 to 7.85×10^{-7} cm^2/s.

TABLE 4 Q_{10} of Mb and free O_2 diffusion in the cell

D_{Mb}	[T_1, T_2], °C	[20, 30]	[25, 35]	[30, 40]	[35, 45]
	Q_{10}	1.51	1.41	1.34	1.29
K_0*	[T_1, T_2], °C	[22.8, 37]			
	Q_{10}	1.56			

Regression analysis of the temperature-dependent D_{Mb} data gives a linear equation $D_{Mb} = cT - 1.00 \times 10^{-7}$ cm^2/s. The slope c is 2.41×10^{-8} cm^2/s °C. Q_{10} is the relative change in the diffusion coefficient corresponding to 10°C change in temperature as defined by $Q_{10} = (D_2/D_1)^{(10/(T_2-T_1))}$.
*Values extrapolated from literature data (38).

Averaged translational diffusion coefficients

The literature has reported cellular D_{Mb} estimates ranging from 1.2–23 $\times 10^{-7}$ cm^2/s, in contrast to the D_{Mb} of 5–7 $\times 10^{-7}$ cm^2/s at 20°C for 18 g/dl Mb (12,43,44). In rat skeletal muscle homogenate and isolated fiber, metMb exhibits a D_{Mb}, 1.2–1.5 $\times 10^{-7}$ cm^2/s at ~20°C (13,14). FRAP experiments have measured a D_{Mb} of 1.7–2.2 $\times 10^{-7}$ cm^2/s at 37°C following the diffusion of a microinjected horse metMb conjugated with a fluorescence dye in isolated

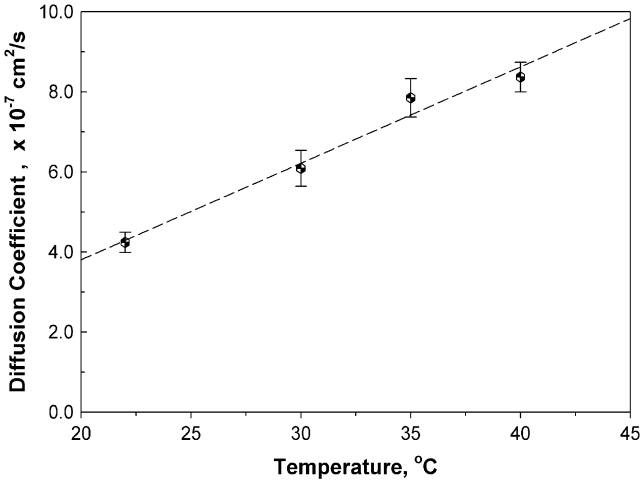

FIGURE 4 Plot of MbO_2 diffusion coefficient versus temperature (°C): The MbO_2 diffusion coefficient in tissue increases proportionally as temperature rises. Regression analysis of the temperature-dependent D_{Mb} data gives a linear equation with an $R^2 = 0.986$ within the temperature range of 22°C–40°C. The slope is 2.41×10^{-8} cm^2/s °C.

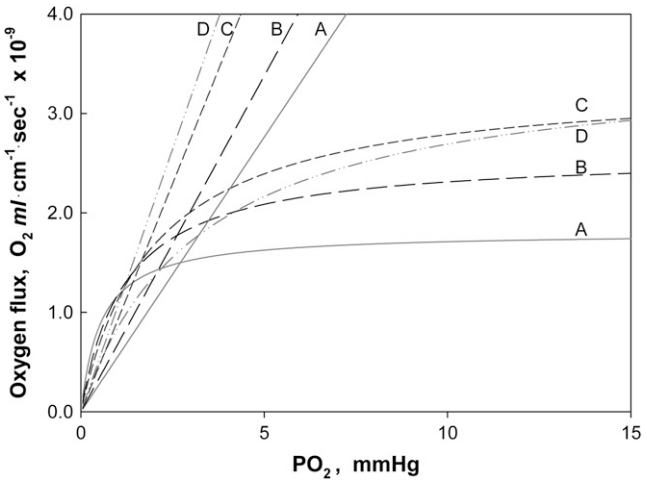

FIGURE 5 Plot of Mb-facilitated O_2 diffusion versus free O_2 flux as a function of PO_2 at different temperatures: The equation $FO_2^{O_2} = K_0 PO_2$ describes the linear rise of free O_2 flux with PO_2. Krogh's diffusion coefficient, K_0, is the proportionality constant and the slope. Four straight lines reveal the rate of change at different K_0 values: *A*) 2.52×10^{-5} ml O_2 cm^{-1}min^{-1}atm^{-1} at 23°C, *B*) 3.08×10^{-5} ml O_2 cm^{-1}min^{-1}atm^{-1} at 30°C, *C*) 4.18×10^{-5} ml O_2 cm^{-1}min^{-1}atm^{-1} at 34.2°C, and *D*) 4.81×10^{-5} ml O_2 cm^{-1}min^{-1}atm^{-1} at 40.4°C. The equation $FO_2^{Mb} = D_{Mb}C_{Mb}(PO_2/(PO_2+P50))$ describes the Mb-facilitated O_2 diffusion as a function of PO_2, P50, C_{Mb}, and D_{Mb} and gives rise to a set of nonlinear curves. The PO_2 corresponding to the condition, $FO_2^{O_2} = FO_2^{Mb}$, denotes the equipoise diffusion PO_2. Temperature affects both D_{Mb} and P_{50} and consequently the O_2 flux contribution from Mb-facilitated diffusion at *A*) 22°C, *B*) 30°C, *C*) 35°C, and *D*) 40°C.

muscle fiber (16,17). According to the FRAP experiments, cellular Mb diffuses 10 times slower than dilute Mb solution.

Even though the fluorescence recovery experiments yield a cellular D_{Mb}, the uncertain contribution of metMb reaction kinetics with Mb reductase, the nonphysiological nature of an isolated fiber model, and differential bound and free metabolite pool in homogenate versus in the cell raise questions about the validity of the FRAP determined D_{Mb} in respiring tissue (18,45). According to the NMR analysis, Mb diffusion in respiring tissue slows to ~48% of the solution state value at 35°C. Mb diffuses 3.6 times faster than the Mb mobility determined by FRAP.

Rotational diffusion plays a very minor role in facilitating O_2 transport, since O_2 remains bound during the correlation time and does not move a significant distance (46,47).

D_{Mb} and Mb contribution to O_2 flux

The D_{Mb} and K_0 provide a means to partition the contribution from free O_2 and MbO_2. K_0 depends upon temperature and has reported values ranging from 2.52 to 4.81×10^{-5} ml O_2 cm^{-1}min^{-1}atm^{-1} (38). With a K_0 of 4.18×10^{-5} ml O_2 cm^{-1}min^{-1}atm^{-1}, a P50 of 1.98 mmHg, and a myocardium Mb concentration of 0.19 mM, the averaged cellular D_{Mb} of 7.85×10^{-7} cm^2/s yields a equipoise diffusion PO_2 of 1.67 mmHg. Below a PO_2 of 1.67 mmHg, the Mb-dependent contribution to the O_2 flux begins to dominate.

TABLE 5 Equipoise diffusion PO_2 in heart and skeletal at different temperatures

	Temperature (°C)			
	22*	30	35	40
K_0 (ml O_2 cm^{-1} × min^{-1} . atm^{-1}) × 10^{-5}	2.52	3.08	4.18	4.81
P50 (mmHg)†	0.55	1.21	1.98	3.23
D_{Mb} (cm^{2}s^{-1}) ×10^{-7}	4.24	6.09	7.85	8.37
D_{Mb} C_{Mb}(cm^{2}s^{-1} mM) × 10^{-7} myocardium‡	0.81	1.16	1.49	1.59
D_{Mb} C_{Mb}(cm^{2}s^{-1} mM) × 10^{-7} skeletal muscle‡	1.79	2.56	3.29	3.54
Equipoise diffusion PO_2 (mmHg) myocardium	2.72	2.63	1.67	0.15
Equipoise diffusion PO_2 (mmHg) skeletal muscle	6.67	7.27	6.08	4.24

*Actual temperature for K_0 measurements: 23°C, 30°C, 34.2°C, 40.4°C (38).

†P50 calculated from the equation P50 = $e^{0.098T-2.748}$, where T is in °C (49). Experimentally determined P50 of 1.5 mmHg at ~25°C and K_0 = 2.52×10^{-5} ml O_2 cm^{-1} × min^{-1} × atm^{-1} yields equipoise diffusion PO_2 1.77 mmHg for myocardium and 5.72 for skeletal muscle (10,74).

‡Mb concentration in rat myocardium assumed as 0.19 mM and 0.42 mM in rat skeletal muscle (10).

Given that sufficient O_2 exists to saturate Mb > 90% in the basal state, the basal PO_2 must stand poised well above 10 mmHg. Even with increased workload and respiration, in vivo myocardium experiments have not detected partial O_2 saturation of Mb (23,25,48). No transient fluctuation in MbO_2

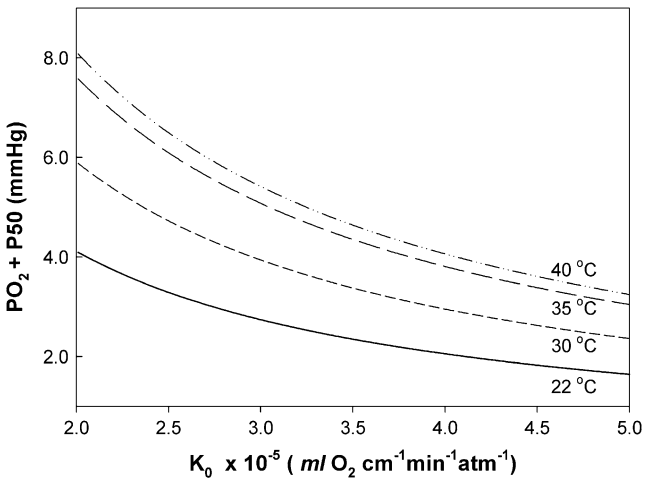

FIGURE 6 Plot of K_0 versus (PO_2 + P50) based on the equation $K_0 = (D_{Mb}C_{Mb}/(PO_2+P50))$ under the condition $(FO_2^{Mb}/FO_2^{O_2}) = 1$. K_0 shows a hyperbolic relationship with (PO_2 + P50), given a C_{Mb} of 0.19 mM and D_{Mb} (Table 2). Since K_0, D_{Mb}, and P50 depend upon temperature, different graphs reflect the hyperbolic relationship at 22°C, 30°C, 35°C, and 40°C. The graph accommodates the broad range of literature reported P50 and K_0 values. At ~22°C, the Mb P50 value can vary from 0.55 to 2.3 mmHg, whereas the K_0 values can vary from $2.52-4.28 \times 10^{-5}$ ml O_2 cm^{-1} × min^{-1} × atm^{-1}.

saturation appears over the cardiac contraction cycle (33). In the basal state myocardium at 35°C, Mb does not play a significant role in regulating respiration under normoxic conditions.

As temperature increases from 22°C to 40°C, myocardial function and Mb diffusion increase. Mb P50 rises from 0.55 to 3.23 mmHg; D_{Mb} increases from 4.24 to 8.37×10^{-7} cm^2/s. The increased Mb diffusion with temperature enhances its ability to transport O_2.

However, the contribution of free O_2 flux also increases linearly with PO_2 and K_0. K_0 increases from 22°C to 40°C (2.52, 3.08, 4.18, and 4.81×10^{-5} ml O_2 $cm^{-1}min^{-1}atm^{-1}$). Moreover, P50 also increases from 0.55 to 3.23, extrapolated from equation of temperature-dependent Mb P50 (49). The competing effects of K_0 and P50 versus D_{Mb} create a decrease in the equipoise diffusion PO_2 from 2.72 to 0.15 mmHg in myocardium as tissue temperature rises. A similar trend appears in skeletal muscle.

A definitive equipoise diffusion PO_2 analysis requires firm experimental K_0 and P50 values. Unfortunately, the literature contains a range of P50 and K_0 values, especially with respect to temperature. For Mb P50, the values can vary from 0.55 to 1.5 mmHg at 25°C (10,49). For K_0, the values also vary widely (38). At a given P50 value, an increase in the experimentally determined K_0 value will decrease the equipoise diffusion PO_2. Similarly, at any given K_0, a rising P50, as observed with increasing temperature, will decrease the equipoise diffusion PO_2.

D_{Mb} and myocardial function

Mb-facilitated diffusion appears to have no significant role in regulating myocardial respiration. In the basal state, in situ myocardium exhibits no detectable ^{1}H-NMR signal of the deoxy Mb proximal histidyl $N_\delta H$ proton (23,25,48). The basal PO_2 must then saturate over 90% of MbO_2. With Mb p50 of 2.3 at 37°C, the basal PO_2 exceeds 10 mmHg. Even when myocardial respiration increases by a factor of 2 in the in situ myocardium, NMR still cannot detect any deoxy Mb signal. Certainly, in whole animals, myocardial work can increase 5 times above the basal level. However, if Mb does not desaturate as work increases 2 times above the basal level, increasing the work 2.5 times more would probably still not drop the PO_2 from >10 mmHg to the equipoise diffusion PO_2 of 1.67 mmHg, in which Mb can begin to contribute significantly to the O_2 flux.

The O_2 saturation state of the residual 10% of the MbO_2 reflects a measurement uncertainty and not the presence of any partially saturated MbO_2 pool. Given the signal to noise and baseline contribution, rigorous NMR spectral interpretation usually avoids ascribing statistical significance to any peak that has a 1.1:1.0 signal/noise ratio, especially with respect to calculating a PO_2 in the basal state from a hyperbolic relationship describing O_2 binding to Mb. With PO_2 well above the P50, a small change in the deoxy Mb signal intensity can correspond nonlinearly to a large change in the PO_2. Even if the cell contains a 10% partially saturated Mb pool, such a small pool would permit only 10% of the Mb to contribute to the O_2 flux and decrease dramatically the equipoise diffusion PO_2.

The insignificant contribution of Mb to myocardial O_2 flux agrees with Mb inactivation studies (36,41). Under a range of normoxic, hypoxic, and work conditions, acute CO inactivation of up to 80% of Mb in the myocardium produces no respiratory, contractile, or metabolic alteration in the myocardium. Even under conditions that should accentuate the purported Mb-facilitated O_2 diffusion, Mb inactivation still does not trigger any significant physiological response (36,41).

D_{Mb} and skeletal muscle function

In human skeletal muscle, most NMR studies have also not detected the proximal histidyl $N_\delta H$ signal of deoxy Mb in the resting state, consistent with a PO_2 above 10 mmHg (24,50,51). Only one recent study has invoked the increased sensitivity of a 4 T (Tesla) magnetic field over 1.5–2 T used in previous experiments to claim the detection of a deoxy Mb signal in resting muscle, ascribed to a PO_2 of 34 mmHg (52). The primary spectral evidence, however, appears quite poor and unconvincing. Moreover, the purported sensitivity enhancement of 4 T over 1.5–2 T overlooks the reported sensitivity loss arising from field-dependent relaxation of the deoxy Mb proximal histidyl $N_\delta H$ signal, which broadens the line width and decreases the signal to noise with a quadratic dependence on field (20). Nevertheless, in all cases, given the equipoise diffusion PO_2 of 4.24 mmHg at 40°C, Mb has no significant contribution to O_2 flux in the resting state of skeletal muscle.

As muscle starts to contract, however, Mb desaturates rapidly and reaches within ~30 s a steady-state level (24,50). In one report, the steady-state Mb desaturation level declines from 30% to 48% as work in the gastrocnemius muscle increases from 7.8 to 15.1 W (24). In another report, Mb desaturation in exercising quadriceps reaches a steady-state level of ~50% and does not change as work increase from 50% to 100% of VO_{2max} (50). A simple reconciliation of the discordant observations has focused just on the different exercise protocol and intensity (53). The D_{Mb}, however, casts another perspective.

With muscle contraction, the rising energy demand decreases the intracellular PO_2 and can confer an increasing role for Mb-facilitated diffusion. However, the intracellular PO_2 must fall from 10 mmHg or precipitously from 34 mmHg to reach a level of 4.24 mmHg, just above the P50 of 3.23 mmHg at 40°C, before Mb contributes equally with free O_2 to the overall O_2 flux. Mb desaturation coincides with the notion that Mb-facilitated diffusion predominates and rises when muscle contraction energy demands more O_2 flux to meet the rising VO_2.

A constant Mb desaturation from 50% to 100% VO_{2max}, however, fixes the intracellular PO_2 at a certain level. That, then, defines correspondingly a constant contribution from Mb-facilitated diffusion. The constant PO_2 implies an unchanging intracellular gradient. According to Eq. 5, the intracellular O_2 flux depends upon a PO_2 gradient $(d(PO_2)/dx)$. The integration of Eq. 5 across an unchanging dimension from the sarcolemma to the mitochondria will yield a constant PO_2 associated with a constant level of Mb desaturation. But the same intracellular gradient also governs free O_2 diffusion. Regardless of the increase in conductive or convective diffusion, the intracellular O_2 gradient cannot enhance either the Mb or free O_2 flux to match the rising O_2 demand with work. So explaining away the discordant observations of Mb desaturation as a consequence of light versus heavy workload skirts a fundamental question about the impact of the intracellular O_2 gradient in controlling the intracellular O_2 flux. Certainly additional experiments must continue to clarify this.

Transient versus steady state

The role of Mb may vary dramatically in different tissues and in different organisms. Mb concentration appears to confer a different role in myocardium versus skeletal muscle. In marine mammalian muscle, the high Mb concentration leads to a very high equipoise diffusion PO_2 and confirms a prominent role for Mb to serve as an O_2 depot and as a significant transporter of O_2 (3). In seal muscle, the 4 mM Mb concentration raises the equipoise diffusion PO_2 to 67 mmHg. Mb-facilitated diffusion predominates under all physiological conditions.

Mb kinetics experiments cast another perspective on Mb function. At the beginning of muscle contraction, Mb releases rapidly its O_2 store and deoxygenates within ~30 s to a steady-state level (24,54). Focusing only the steady-state changes in Mb desaturation would miss the rapid kinetics that implicate a role for Mb to catalyze the bioenergetics transition from rest to work (33,55).

Isotropic versus anisotropic diffusion

The assessment of Mb contribution to O_2 transport with an averaged D_{Mb} assumes isotropic diffusion. Because the muscle fiber has a longer axial than radial dimension, the diffusion paths should differ correspondingly. Given nonuniform distribution of subcellular structures and the attendant anisotropic tortuosity in the sarcoplasm, the expected D_{Mb} anisotropy can alter the equipoise diffusion PO_2 analysis (13,18). Indeed, researchers have ascribed anisotropic diffusion to PCr and ATP in the sarcoplasm (56).

For Mb, under temperature conditions from 22°C to 35°C, the translational diffusion shows no orientation preference. At 35°C, Mb exhibits an averaged D_{Mb} of $7.85 \pm 0.49 \times 10^{-7}$ cm^2/s mobility. In the X, Y, and Z directions, the Mb diffuses at 7.97 ± 1.03, 7.76 ± 0.68, and $7.85 \pm 0.79 \times 10^{-7}$ cm^2/s, respectively. FRAP experiments have also not discerned any diffusion anisotropy (17).

The NMR determined cellular D_{Mb} of 4.24×10^{-7} cm^2/s at 25°C agrees well with the isotropic rotational diffusion analysis (20). In the field-dependent measurements to determine the rotational correlation time (τ_r) of Mb in solution ($9.7 \pm 0.3 \times 10^{-9}$ s) and in perfused myocardium ($13.6 \pm 1.3 \times 10^{-9}$ s), the 1.4 time increase in the τ_r corresponds most likely to a comparable increase in the cellular microviscosity, based on the Stokes-Einstein relationship. If the solution and cellular molecular hydrodynamics behave identically and if unrestricted diffusion exists, then the increased viscosity and the solution D_{Mb} of $5–7 \times 10^{-7}$ cm^2/s at 20°C for 18 g/dl Mb lead to an estimated cellular D_{Mb} of $3.6–5.0 \times 10^{-7}$ cm^2/s (12,43,44).

In contrast to the D_{Mb} (1.7×10^{-7} cm^2/s at 37°C) determined in FRAP experiments using microinjected metMb with an attached fluorophore, the D_{Mb} (7.85×10^{-7} cm^2/s at 35°C), derived from NMR translational diffusion analysis, shows a much higher Mb diffusion mobility in respiring myocardium (16).

At this time, measurements cannot follow Mb diffusion over a long observation time to detect any restricted diffusion boundaries. For NMR, the available spectrometer has an insufficient detection sensitivity limit to overcome the relaxation losses to observe diffusion or a longer RMS displacement. Such observations would clarify the dimensions of the restricted diffusion boundaries and define any diffusion anisotropy.

RMS displacement

To assess the RMS displacement of Mb, previous studies have used the O_2 off rate constant for MbO_2 of 12 s^{-1} to obtain a $t_{1/2}$ of 58 ms at 20°C (6,57). The displacement reflects the effective Mb diffusion distance before it loses one-half of its O_2. Given D_{Mb} of 4.24×10^{-7} cm^2/s, the Einstein-Smoluchowski equation, $\langle r^2 \rangle = 6$ Dt, yields an RMS displacement of $\langle r \rangle = 3.8$ μm (6). The analysis approach would predict a $\langle r \rangle = 96$ μm for MbCO, given a CO off rate constant of 19×10^{-3} s^{-1} (58). Both MbCO and MbO_2, however, exhibit a similar diffusion coefficient, 11.6×10^{-7} cm^2/s at 22°C.

Another approach to estimate the RMS displacement uses the PGSTE pulse train interval, $\Delta = 24$ ms. Such analysis reveals an $\langle r \rangle = 2.5–3.5$ μm from 22°C to 40°C. Within 2.5–3.5 μm, the data do not indicate any diffusion restriction imposed by subcellular organelles or macromolecules. The insufficient signal sensitivity of the available spectrometer precludes measurements in this study at longer PGSE time intervals that can determine the restricted diffusion boundary. However, according to previous studies of PCr and ATP diffusion in muscle cell, the unrestricted displacement extends radially 8–11 μm from the longitudinal fiber axis

and circumscribes a cylindrical boundary that demarcates unrestricted from restricted diffusion (56,59).

Since muscle cells have a typical dimension of 10×100 μm, the $\langle r \rangle$ of 2.5–3.5 μm represents a small portion of the cell and stays well within the unrestricted diffusion region (60). Moreover, electron microscopy analysis has revealed that many mitochondria cluster near the capillary and form a reticulum. Within an RMS displacement of 2.5–3.5 μm, Mb encounters no diffusion barrier to O_2 delivery (61). Any limitation in the contribution of Mb to the overall O_2 flux must arise from the interaction of microviscosity on Mb mobility.

Cytoplasmic property and architecture

Both the translational and rotational diffusion analyses point to a local cellular environment that slows Mb diffusion. Cellular Mb exhibits a rotational diffusion ~1.4 slower than solution Mb (20). Translational diffusion shows a decrease from 11.6 to 4.24×10^{-7} cm^2/s at 22°C, 2.7 times slower. The observation stands in excellent agreement with the fluorescence diffusion measurements. Relative to the diffusion in saline solution, green fluorescent protein in the cytoplasm exhibits rotational (1.5 times) and translational diffusion (3.2 times) times slower than in saline solution (62). Moreover, parvalbumin diffuses out of frog skinned fibers with an isotropic, averaged diffusion coefficient of $3.74 \pm 0.81 \times 10^{-7}$ cm^2/s at 4°C, also ~1/3 the solution diffusion rate (63). These observations do not agree with the reported 10 time decrease in the cytoplasmic D_{Mb} (16). The discrepancy may arise from model-dependent difference that affects the cellular volume (62).

The decreased diffusion in the cytoplasm can originate from increased cellular viscosity, tortuosity, and protein interaction with the cytomatrix or diffusible particles. If only viscosity contributes to the decrease in Mb mobility, then the relative D_{Mb} in solution and in the cell yields an estimate of the relative viscosity change. Based on H_2O or dilute solution Mb viscosity of 0.95 cP (centipoise) at 22°C, the cellular viscosity must reach 2.6 cP, about a 2.74 increase in viscosity, to account for the observed D_{Mb} (64). FRAP experiments have also determined a cellular viscosity between 2–3 cP (65).

However, the viscosity values predicted by the rotational diffusion measurements appears 2 times smaller. Part of the discordance may arise from the assumptions underlying the derivation of the Stokes-Einstein equation, which expresses a linear relationship between the rotational correlation time and viscosity. The derivation assumes a Brownian particle moving in an ideal, homogeneous, and isotropic solvent. Given an extremely small solvent particle size, classical hydrodynamics then just regards the solvent as continuum. Unfortunately, the cytosol contains a dispersion of large molecular weight cosolutes, such as proteins and ribosomes. The solvent no longer acts as a continuous medium. These cosolutes can disrupt assumptions leading to a linear relationship between correlation time and viscosity. Indeed, recent studies have demonstrated that the microviscosity experienced by a particle in the cell exhibits a power dependence with respect to the bulk viscosity, $(\mu/\mu_0) = ((\eta/\eta_0))^q$, where μ and μ_0 represent the microviscosity in the cell and in the reference state, respectively; η and η_0 represent the bulk viscosity in the cell and in the reference state, respectively. Based on the viscosity $\frac{\eta}{\eta_0} = 3$ predicted by cell models and a reported estimate of $q \sim 0.3$, $\frac{\mu}{\mu_0} = 1.4$. The calculated microviscosity value matches the relative microviscosity of 1.4 derived from the rotational diffusion measurements (66,67). Such a perspective agrees with the premise that viscosity instead of tortuosity or macromolecular interaction contributes predominantly to the decreased Mb diffusion in the cytoplasm. Additional insights on the cellular microviscosity derived from rotational and translational diffusion measurements await further theoretical clarification.

The temperature-dependent change in D_{Mb} and the attendant alteration of viscosity shed additional insight into the current models of the cytoplasm. These models envision the cytoplasm as a concentrated macromolecular solution, a rigid gel network, or an entangled filament network. Distinguishing these different models requires diffusion measurement and modeling of different size molecular probes. As the molecule size increases, a gel network will permit molecular movement until the molecule reaches a percolation cutoff size. Above the percolation cutoff, the probe becomes trapped in the finite volumes of the network. A concentrated macromolecular solution has no percolation cutoff as molecular radius increases. All cytoplasm models, however, envision proteins diffusing at least three times slower in the cell than in solution (27).

Mb diffuses in the cell slightly faster than the value predicted by the cytoplasm models. Its diffusion property casts a perspective on the postulated gel network model. In such a model, the observed D_{Mb} would indicate a percolation cutoff that must exceed 17.5 Å, the hydrodynamic molecular diameter of Mb (26). It is much larger than expected. Without such a large cutoff size, the NMR data would reveal compartmentalization and restricted diffusion. Any cellular network does not impede significantly the mobility of a monomeric 17-kD protein.

Given that both Mb and a 0.5-kD molecular probe diffuse 3 times slower in the cell than in solution, cellular crowding also cannot impose a significant diffusion barrier within an ~2.5–3.5 μm RMS displacement (68). Indeed, the NMR determined Mb rotational diffusion and the Val E11 line width argue for a local fluid phase that approximates water, in agreement with recent time-resolved fluorescence anisotropy measurements of the cell fluid phase viscosity (28,69, 70). The mobility of cellular Mb raises a question about the impact of any postulated cellular crowding on chemical reactions, such as the ones maintaining metabolic homeostasis (71–73).

Finally, the Q_{10} analysis yields another perspective. Because the Q_{10} of Mb diffusion in the cell from 25°C to 35°C (1.41) approximates the corresponding Q_{10} of solution Mb (1.31), no temperature-dependent alteration of the postulated gel phase in the cell has any significant impact on the Mb or monomeric protein mobility.

CONCLUSION

The averaged translational Mb diffusion coefficient of 4.24–8.37 $\times$ 10^{-7} cm^2/s, Mb concentration, P50, and K_0 lead to the determination of equipoise diffusion PO_2 values, which indicate that Mb has no significant role in facilitating O_2 transport in myocardium, has a potential role in skeletal muscle, especially during the onset of contraction and only if PO_2 falls significantly and plays a dominant role for Mb-facilitated diffusion in marine mammals with high Mb concentration in their muscle. The diffusion data also indicate that any postulated cellular gel network must have a percolation cutoff larger than 17.5 Å.

We gratefully acknowledge the invaluable technical assistance of Drs. Jeff Walton and Jeff de Ropp.

We gratefully acknowledge funding support from the National Institutes of Health GM 58688 (T.J.), Philip Morris 005510 (T.J.), and American Heart Association Western States Affiliate 0265319Y (U.K.).

REFERENCES

1. Wittenberg, B. A., and J. B. Wittenberg. 1989. Transport of oxygen in muscle. *Annu. Rev. Physiol.* 51:857–878.
2. Guyton, G. P., K. S. Stanek, R. C. Schneider, P. W. Hochachka, W. E. Hurford, D. G. Zapol, G. C. Liggins, and W. M. Zapol. 1995. Myoglobin saturation in free-diving Weddell seals. *J. Appl. Physiol.* 79:1148–1155.
3. Ponganis, P. J., U. Kreutzer, N. Sailasuta, T. Knower, R. Hurd, and T. Jue. 2002. Detection of myoglobin desaturation in Mirounga angustirostris during apnea. *Am. J. Physiol. Regul. Integr. Comp. Physiol.* 282:R267–R272.
4. Gimenez, M., R. J. Sanderson, O. K. Reiss, and N. Banchero. 1977. Effects of altitude on myoglobin and mitochondrial protein in canine skeletal muscle. *Respiration.* 34:171–176.
5. Terrados, N., E. Jansson, C. Sylven, and L. Kaijser. 1990. Is hypoxia a stimulus for synthesis of oxidative enzymes and myoglobin? *J. Appl. Physiol.* 68:2369–2372.
6. Wittenberg, J. B., and B. A. Wittenberg. 2003. Myoglobin function reassessed. *J. Exp. Biol.* 206:2011–2020.
7. Chung, Y., and T. Jue. 1996. Cellular response to reperfused oxygen in the postischemic myocardium. *Am. J. Physiol.* 271:H687–H695.
8. Garry, D. J., G. A. Ordway, J. N. Lorenz, N. B. Radford, E. R. Chin, R. W. Grange, R. Bassel-Duby, and R. S. Williams. 1998. Mice without myoglobin. *Nature.* 395:905–908.
9. Godecke, A., U. Flogel, K. Zanger, Z. Ding, J. Hirchenhain, U. K. Decking, and J. Schrader. 1999. Disruption of myoglobin in mice induces multiple compensatory mechanisms. *Proc. Natl. Acad. Sci. USA.* 96:10495–10500.
10. Wittenberg, J. B. 1970. Myoglobin-facilitated oxygen diffusion: role of myoglobin in oxygen entry into muscle. *Physiol. Rev.* 50:559–636.
11. Johnson, R. L., G. J. F. Heigenhauser, C. C. W. Hsia, N. L. Jones, and P. D. Wagner. 1996. Determinants of gas exchange and acid-base balance during exercise. *In* Exercise: Regulation and Integration of Multiple Systems. L. B. Rowell and J. T. Shepher, editors. Oxford University Pres, New York. 515–584.
12. Riveros-Moreno, V., and J. B. Wittenberg. 1972. The self-diffusion coefficients of myoglobin and hemoglobin in concentrated solution. *J. Biol. Chem.* 247:895–901.
13. Baylor, S. M., and P. C. Pape. 1988. Measurement of myoglobin diffusivity in the myoplasm of frog skeletal muscle fibres. *J. Physiol.* 406:247–275.
14. Moll, W. 1968. The diffusion coefficient of myoglobin in muscle homogenate. *Pflug. Arch. Ges. Physiol. Mensch. Tiere.* 299:247–251.
15. Verkman, A. S. 2003. Diffusion in cells measured by fluorescence recovery after photobleaching. *Methods Enzymol.* 360:635–648.
16. Jurgens, K. D., T. Peters, and G. Gros. 1994. Diffusivity of myoglobin in intact skeletal muscle cells. *Proc. Natl. Acad. Sci. USA.* 91:3829–3833.
17. Papadopoulos, S., V. Endeward, B. Revesz-Walker, K. D. Jurgens, and G. Gros. 2001. Radial and longitudinal diffusion of myoglobin in single living heart and skeletal muscle cells. *Proc. Natl. Acad. Sci. USA.* 98:5904–5909.
18. Groebe, K. 1995. An easy-to-use model for O2 supply to red muscle. Validity of assumptions, sensitivity to errors in data. *Biophys. J.* 68: 1246–1269.
19. Livingston, D. J., G. N. La Mar, and W. D. Brown. 1983. Myoglobin diffusion in bovine heart muscle. *Science.* 220:71–73.
20. Wang, D., U. Kreutzer, Y. Chung, and T. Jue. 1997. Myoglobin and hemoglobin rotational diffusion in the cell. *Biophys. J.* 73:2764–2770.
21. Kreutzer, U., D. S. Wang, and T. Jue. 1992. Observing the ^{1}H NMR signal of the myoglobin Val-E11 in myocardium: an index of cellular oxygenation. *Proc. Natl. Acad. Sci. USA.* 89:4731–4733.
22. Stejskal, E. O., and J. E. Tanner. 1965. Spin diffusion measurements: spin echoes in the presence of a time-dependent field gradient. *J. Chem. Phys.* 42:288–292.
23. Kreutzer, U., Y. Mekhamer, T. K. Tran, and T. Jue. 1998. Role of oxygen in limiting respiration in the in situ myocardium. *J. Mol. Cell. Cardiol.* 30:2651–2655.
24. Mole, P. A., Y. Chung, T. K. Tran, N. Sailasuta, R. Hurd, and T. Jue. 1999. Myoglobin desaturation with exercise intensity in human gastrocnemius muscle. *Am. J. Physiol.* 277:R173–R180.
25. Zhang, J., Y. Murakami, Y. Zhang, Y. Cho, Y. Ye, G. Gong, R. Bache, K. Ugurbil, and A. H. L. From. 1999. Oxygen delivery does not limit cardiac performance during high work states. *Am. J. Physiol.* 276: H50–H57.
26. Kataoka, M., I. Nishii, T. Fujisawa, T. Ueki, F. Tokunaga, and Y. Goto. 1995. Structural characterization of the molten globule and native states of apomyoglobin by solution x-ray-scattering. *J. Mol. Biol.* 249:215–228.
27. Luby-Phelps, K., F. Lanni, and D. L. Taylor. 1988. The submicroscopic properties of cytoplasm as a determinant of cellular function. *Annu. Rev. Biophys. Biophys. Chem.* 17:369–396.
28. Seksek, O., J. Biwersi, and A. S. Verkman. 1997. Translational diffusion of macromolecule-sized solutes in cytoplasm and nucleus. *J. Cell Biol.* 138:131–142.
29. Torrey, H. C. 1956. Bloch equations with diffusion terms. *Phys. Rev.* 104:563–565.
30. Nicolay, K., K. P. J. Braun, R. A. de Graaf, R. M. Dijkhuizen, and M. J. Kruiskamp. 2001. Diffusion NMR spectroscopy. *NMR Biomed.* 14: 94–111.
31. Basser, P. J., J. Mattiello, and D. LeBihan. 1994. Estimation of the effective self-diffusion tensor from the NMR spin-echo. *J. Magn. Reson.* 103:247–254.
32. Kreutzer, U., Y. Chung, D. Butler, and T. Jue. 1993. ^{1}H-NMR characterization of the human myocardium myoglobin and erythrocyte hemoglobin signals. *Biochim. Biophys. Acta.* 1161:33–37.
33. Chung, Y., and T. Jue. 1999. Regulation of respiration in myocardium in the transient and steady state. *Am. J. Physiol.* 277:H1410–H1417.

34. Kreutzer, U., and T. Jue. 2004. The role of myoglobin as a scavenger of cellular NO in myocardium. *Am. J. Physiol.* 286:H985–H991.
35. Price, W. S. 1997. Pulsed-field gradient nuclear magnetic resonance as a tool for studying translational diffusion. 1. Basic theory. *Concepts Magn. Reson.* 9:299–336.
36. Chung, Y., S. J. Huang, and A. Glabe. 2006. Impact of myoglobin inactivation on myocardial function. *Am. J. Physiol.* 290:C1616–C1624.
37. Haase, A., J. Frahm, W. Hanicke, and D. Matthaei. 1985. ^{1}H NMR chemical-shift selective (chess) imaging. *Phys. Med. Biol.* 30:341–344.
38. Bentley, T. B., H. Meng, and R. N. Pittman. 1993. Temperature-dependence of oxygen diffusion and consumption in mammalian striated-muscle. *Am. J. Physiol.* 264:H1825–H1830.
39. Laster, S. B., L. C. Becker, G. Ambrosio, and W. E. Jacobus. 1989. Reduced aerobic metabolic efficiency in globally ''stunned'' myocardium. *J. Mol. Cell. Cardiol.* 21:419–426.
40. Kreutzer, U., and T. Jue. 1995. Critical intracellular oxygen in the myocardium as determined with the ^{1}H NMR signal of myoglobin. *Am. J. Physiol.* 268:H1675–H1681.
41. Glabe, A., Y. Chung, D. Xu, and T. Jue. 1998. Carbon monoxide inhibition of regulatory pathways in myocardium. *Am. J. Physiol.* 274:H2143–H2151.
42. Schenkman, K. A., D. A. Beard, W. A. Ciesielski, and E. O. Feigl. 2003. Comparison of buffer and red blood cell perfusion of guinea pig heart oxygenation. *Am. J. Physiol. Heart Circ. Physiol.* 285:H1819–H1825.
43. Federspiel, W. J. 1986. A model study of intracellular oxygen gradients in a myoglobin-containing skeletal muscle fiber. *Biophys. J.* 49:857–868.
44. Papadopoulos, S., K. D. Jurgens, and G. Gros. 1995. Diffusion of myoglobin in skeletal muscle cells—dependence on fibre type, contraction and temperature. *Pflugers Arch. Eur. J. Physiol.* 430: 519–525.
45. Iles, R. A., A. N. Stevens, J. R. Griffiths, and P. G. Morris. 1985. Phosphorylation status of the liver by ^{31}P NMR spectroscopy and its implications for metabolic control. *Biochem. J.* 229:141–151.
46. Gros, G., D. Lavalette, W. Moll, H. Gros, B. Amand, and F. Pochon. 1984. Evidence for rotational contribution to protein-facilitated proton transport. *Proc. Natl. Acad. Sci. USA.* 81:1710–1714.
47. Wyman, J. 1966. Facilitated diffusion and the possible role of myoglobin as a transport mechanism. *J. Biol. Chem.* 241:115–121.
48. Kreutzer, U., Y. Mekhamer, Y. Chung, and T. Jue. 2001. Oxygen supply and oxidative phosphorylation limitation in rat myocardium in situ. *Am. J. Physiol. Heart Circ. Physiol.* 280:H2030–H2037.
49. Schenkman, K. A., D. R. Marble, D. H. Burns, and E. O. Feigl. 1997. Myoglobin oxygen dissociation by multiwavelength spectroscopy. *J. Appl. Physiol.* 82:86–92.
50. Richardson, R. S., E. A. Noyszewski, K. Kendrick, J. S. Leigh, and P. D. Wagner. 1995. Myoglobin O_2 desaturation during exercise. Evidence of limited O_2 transport. *J. Clin. Invest.* 96:1916–1926.
51. Wang, Z., E. A. Noyszewski, and J. S. Leigh. 1990. In vivo MRS measurement of deoxymyoglobin in human forearms. *Magn. Reson. Med.* 14:562–567.
52. Richardson, R. S., S. Duteil, C. Wary, D. W. Wray, J. Hoff, and P. Carlier. 2006. Muscle intracellular oxygenation: the impact of ambient of oxygen availability. *J. Physiol.* 571:415–424.
53. Conley, K. E., G. A. Ordway, and R. S. Richardson. 2000. Deciphering the mysteries of myoglobin in striated muscle. *Acta Physiol. Scand.* 168:623–634.
54. Chung, Y., P. A. Mole, N. Sailasuta, T. K. Tran, R. Hurd, and T. Jue. 2005. Control of respiration and bioenergetics during muscle contraction. *Am. J. Physiol. Cell Physiol.* 288:C730–C738.
55. Chung, Y., R. Sharman, R. Carlsen, S. W. Unger, D. Larson, and T. Jue. 1998. Metabolic fluctuation during a muscle contraction cycle. *Am. J. Physiol.* 274:C846–C852.
56. de Graaf, R. A., A. van Kranenburg, and K. Nicolay. 2000. In vivo P-31-NMR diffusion spectroscopy of ATP and phosphocreatine in rat skeletal muscle. *Biophys. J.* 78:1657–1664.
57. Gibson, Q. H., J. S. Olson, R. S. McKinnie, and R. J. Rohlfs. 1986. A kinetic description of ligand binding to sperm whale myoglobin. *J. Biol. Chem.* 261:10228–10239.
58. Carver, T. E., R. E. Brantley Jr., E. W. Singleton, R. M. Arduini, M. L. Quillin, G. N. Phillips Jr., and J. S. Olson. 1992. A novel site-directed mutant of myoglobin with an unusually high O_2 affinity and low autooxidation rate. *J. Biol. Chem.* 267:14443–14450.
59. van Gelderen, P., D. DesPres, P. C. van Zijl, and C. T. Moonen. 1994. Evaluation of restricted diffusion in cylinders. Phosphocreatine in rabbit leg muscle. *J. Magn. Reson. B.* 103:255–260.
60. Arrio-Dupont, M., S. Cribier, G. Foucault, P. F. Devaux, and A. d'Albis. 1996. Diffusion of fluorescently labeled macromolecules in cultured muscle cells. *Biophys. J.* 70:2327–2332.
61. Kirkwood, S. P., E. A. Munn, and G. A. Brooks. 1986. Mitochondrial reticulum in limb skeletal muscle. *Am. J. Physiol.* 251:C395–C402.
62. Swaminathan, R., C. P. Hoang, and A. S. Verkman. 1997. Photobleaching recovery and anisotropy decay of green fluorescent protein GFP-S65T in solution and cells: cytoplasmic viscosity probed by green fluorescent protein translational and rotational diffusion. *Biophys. J.* 72:1900–1907.
63. Maughan, D. W., and R. E. Godt. 1999. Parvalbumin concentration and diffusion coefficient in frog myoplasm. *J. Muscle Res. Cell Motil.* 20:199–209.
64. Lide, D. R., and H. P. R. Frederikse. 1990. CRC Handbook of Chemistry and Physics, 71st ed. CRC Press, Boca Raton, FL.
65. Mastro, A. M., M. A. Babich, W. D. Taylor, and A. D. Keith. 1984. Diffusion of a small molecule in the cytoplasm of mammalian-cells. *Proc. Natl. Acad. Sci. USA.* 81:3414–3418.
66. Lavalette, D., M. A. Hink, M. Tourbez, C. Tetreau, and A. J. Visser. 2006. Proteins as micro viscosimeters: Brownian motion revisited. *Eur. Biophys. J.* 35:517–522.
67. Lavalette, D., C. Tetreau, M. Tourbez, and Y. Blouquit. 1999. Microscopic viscosity and rotational diffusion of proteins in a macromolecular environment. *Biophys. J.* 76:2744–2751.
68. Kao, H. P., J. R. Abney, and A. S. Verkman. 1993. Determinants of the translational mobility of a small solute in cell cytoplasm. *J. Cell Biol.* 120:175–184.
69. Swaminathan, R., S. Bicknese, N. Periasamy, and A. S. Verkman. 1996. Cytoplasmic viscosity near the cell plasma membrane: translational diffusion of a small fluorescent solute measured by total internal reflection-fluorescence photobleaching recovery. *Biophys. J.* 71:1140–1151.
70. Fushimi, K., J. A. Dix, and A. S. Verkman. 1990. Cell membrane fluidity in the intact kidney proximal tubule measured by orientation-independent fluorescence anisotropy imaging. *Biophys. J.* 57:241–254.
71. Goodsell, D. S. 1991. Inside a living cell. *Trends Biochem. Sci.* 16: 203–206.
72. Sumegi, B., A. D. Sherry, C. R. Malloy, C. Evans, and P. A. Srere. 1991. Is there tight channelling in the tricarboxylic acid cycle metabolon? *Biochem. Soc. Trans.* 19:1002–1005.
73. Welch, G. R., and P. R. Marmillot. 1991. Metabolic ''channeling'' and cellular physiology. *J. Theor. Biol.* 152:29–33.
74. Lin, P. C., U. Kreutzer, and T. Jue. 2007. Myoglobin translational diffusion in rat myocardium and its implication on intracellular oxygen transport. J. Physiol. 578:595–603.